THE ASTROPHYSICAL JOURNAL, 542:740–749, 2000 October 20
© 2000. The American Astronomical Society. All rights reserved. Printed in U.S.A.

MULTIWAVELENGTH EXAMINATION OF THE *COS B* FIELD 2CG 075+00 YIELDS A BLAZAR IDENTIFICATION FOR 3EG J2016+3657

R. MUKHERJEE
Department of Physics and Astronomy, Barnard College and Columbia University, New York, NY 10027
E. V. GOTTHELF AND J. HALPERN
Department of Physics and Astronomy, Columbia University, New York, NY 10027
AND
M. TAVANI
Istituto di Fisica Cosmica e Tecnologie Relative, CNR, via Bassini 15, I-20133 Milano, Italy; and Columbia Astrophysics Lab, New York, NY 10027
Received 2000 March 29; accepted 2000 May 26

ABSTRACT

We present a high-energy study of the intriguing *COS B* γ-ray field, 2CG 075+00, in order to search for possible counterparts. New EGRET data show that the *COS B* emission probably corresponds to two localized γ-ray sources, 3EG J2016+3657 and 3EG J2021+3716. Spectral fits to these EGRET sources, assuming a power-law model, yield photon indices of ~ 2 for each object. We examine archival *ROSAT* and *ASCA* X-ray data that overlap both EGRET error boxes and find several point sources in the region to a flux limit of approximately 6.5×10^{-13} ergs cm^{-2} s^{-1}. We conclude that the most probable candidate for 3EG J2016+3657 is the compact, variable, flat-spectrum radio and millimeter source B2013+370 (G74.87+1.22), which has blazarlike properties. The other source, 3EG J2021+3716, remains unidentified.

Subject headings: BL Lacertae objects: general — gamma rays: observations — X-rays: general

1. INTRODUCTION

Since the first surveys of the γ-ray sky with the *COS B* satellite the nature of most γ-ray sources remain a mystery, as few of these sources have firmly established counterparts at any other wave band (Swanenburg et al. 1981). With the launch of the *Compton Gamma Ray Observatory* (*CGRO*) in 1991, improved surveys at relatively higher angular resolution in the γ-ray band were made possible. In particular, a systematic survey of the γ-ray sky, including the *COS B* source regions, was carried out with the onboard EGRET instrument at energies above 100 MeV. EGRET has so far detected 271 sources of high-energy γ-rays in the third EGRET (3EG) catalog (Hartman et al. 1999), of which 169 remain unidentified (74 of these are at $|b| < 10°$), with no convincing counterparts at other wavelengths. Surprisingly, only two of the unidentified *COS B* sources have been subsequently associated with EGRET sources, and both are pulsars, namely, Geminga (Bertsch et al. 1992) and 2CG 342−02 (PSR B1706−44; Thompson et al. 1992). A third source, PSR B1046−58, could possibly be the candidate for identification of 2CG 288−00 (Kaspi et al. 2000).

To date, the only sources of high-energy γ-rays convincingly identified are the blazars at high Galactic latitudes and the pulsars at low latitudes. Studies of individual unidentified EGRET γ-ray source fields have been inconclusive in locating the origins of their emission. Comprehensive surveys of the fields associated with these sources have met with limited success (see Mukherjee, Grenier, & Thompson 1997a for a review). Several researchers have noted that the unidentified EGRET sources in the Galactic plane lie in proximity to star formation sites and supernova remnants (Yadigaroglu & Romani 1997; Sturner & Dermer 1995; Esposito et al. 1996), while others report a correlation with OB associations and massive stars (Kaaret & Cottam 1996; Kaul & Mitra 1997; Romero, Benaglia, & Torres 1999). Efforts to identify the γ-ray sources at other wavelengths include systematic multifrequency radio observations (e.g., Özel et al. 1988) and X-ray imaging studies (e.g., Brazier et al. 1996; 1998; Roberts & Romani 1998; Mirabal et al. 2000).

In this article we revisit the region containing the unidentified *COS B* source 2CG 075+00, located in the Cygnus region, for which a significant amount of archival γ-ray (EGRET) and X-ray (*ASCA* and *ROSAT*) data have accumulated. Previous attempts to locate the origin of the high-energy emission were fraught with frustration, as the position associated with 2CG 075+00 in the second EGRET catalog (Thompson et al. 1995), 2EG J2019+3719, has shifted in the 3EG catalog and has split into two discrete sources, 3EG J2016+3657 and 3EG J2021+3716. Fortunately, both revised EGRET error boxes have overlapping archival *ASCA* and *ROSAT* observations. We now reanalyze the EGRET data along with the corresponding X-ray fields using the refined γ-ray positions from the later catalog.

2. THE γ-RAY OBSERVATIONS

2CG 075+00, first observed by *COS B*, is located in the Galactic plane. The revised *COS B* position for the source is $l = 76.^{\circ}1$, $b = 0.^{\circ}5$, with an error radius of $\sim 1.^{\circ}0$ (Pollock et al. 1985). In the Second *COS B* Catalog, Swanenburg et al. (1981) note that the source structure could possibly be interpreted as containing extended features. The integrated γ-ray flux from the source at energies greater than 100 MeV was found to be 1.3×10^{-6} photons cm^{-2} s^{-1}, although no spectral information was available (Swanenburg et al. 1981).

Since its launch in 1991, EGRET has observed the error circle of 2CG 075+00 several times. EGRET is sensitive to γ-rays in the energy range from 30 MeV to 30 GeV, with a point source sensitivity of $\sim 3 \times 10^{-7}$ photons cm^{-2} s^{-1} (>100 MeV). It has an effective area of 1.5×10^{3} cm^{2} in the energy range 0.2–1 GeV, decreasing to about one-half the

on-axis value at 18° off-axis and to one-sixth at 30°. The nominal angular resolution is 0.°6 at 500 MeV, improving to 0.°4 at 3 GeV. Details of the instrument preflight and in-flight calibration are described elsewhere (Thompson et al. 1993; Esposito et al. 1999).

In the second EGRET (2EG) catalog, 2CG 075+00 was weakly detected as 2EG J2019+3719. Reanalysis of the region using a larger data set for the 3EG revealed two sources, 3EG J2016+3657 and 3EG J2021+3716, with error radii of 33′ and 18′, respectively, at the 95% contour (Hartman et al. 1999). In the summed Phase 1 through Cycle 4 EGRET observations, 3EG J2016+3657 and 3EG J2021+3716 were detected at the highest significances of 6.4 σ and 10.3 σ, respectively, and these observations were used for the position determination. Figure 1 shows the EGRET source positions superimposed on the *ROSAT* X-ray image that is described in § 3. 3EG J2021+3716 is completely within the error circle of the *COS B* source 2CG 075+00, also shown in Figure 1.

An analysis of 4.5 yr of EGRET data based on photons with energies greater than 1 GeV gives a slightly different result for source positions in the Cygnus region (GeV catalog; Lamb & Macomb 1997). The GeV catalog lists one source with an error circle overlapping that of 2CG 075+00, namely, GEV J2020+3658, at $l = 75.°29$, $b = 0.°24$ (see Fig. 1).

We examined the flux history of 3EG J2016+3657 and 3EG J2021+3716 to search for variability, such as is characteristic of high-latitude EGRET blazars. The light curves for these sources are displayed in Figure 2 using data from the 3EG catalog (Hartman et al. 1999) for the Phase 1–Cycle 4 observations (1991–1995). Two additional observations were made in Cycle 6 in viewing period (VP) 601.1 (1996 October) and VP 623.5 (1997 July). These data were analyzed using the standard EGRET data-processing technique, as described in Mattox et al. (1996) and Hartman et al. (1999), and are included in Figure 2. The horizontal bars on the individual data points denote the extent of the VP for that observation. Fluxes have been plotted for all detections greater than 2 σ. For detections below 2 σ, upper limits at the 95% confidence level are shown. A χ^2 analysis can be used to calculate a variability index according to that defined by McLaughlin et al. (1996). Although somewhat arbitrary, the quantity V can be used to judge the strength of the evidence of flux variability. Following the classification used in McLaughlin et al. (1996), we use $V < 0.5$ to indicate nonvariability and $V \geq 1$ to indicate variability. In this case, we obtain $V = 1.1$ for 3EG J2016+3657 and $V = 1.57$ for 3EG J2021+3716. We note, however, that 3EG J2016+3657 and 3EG J2021+3716 are in a confused region (as indicated in the 3EG Catalog), and the variability numbers could be an artifact of the analysis,

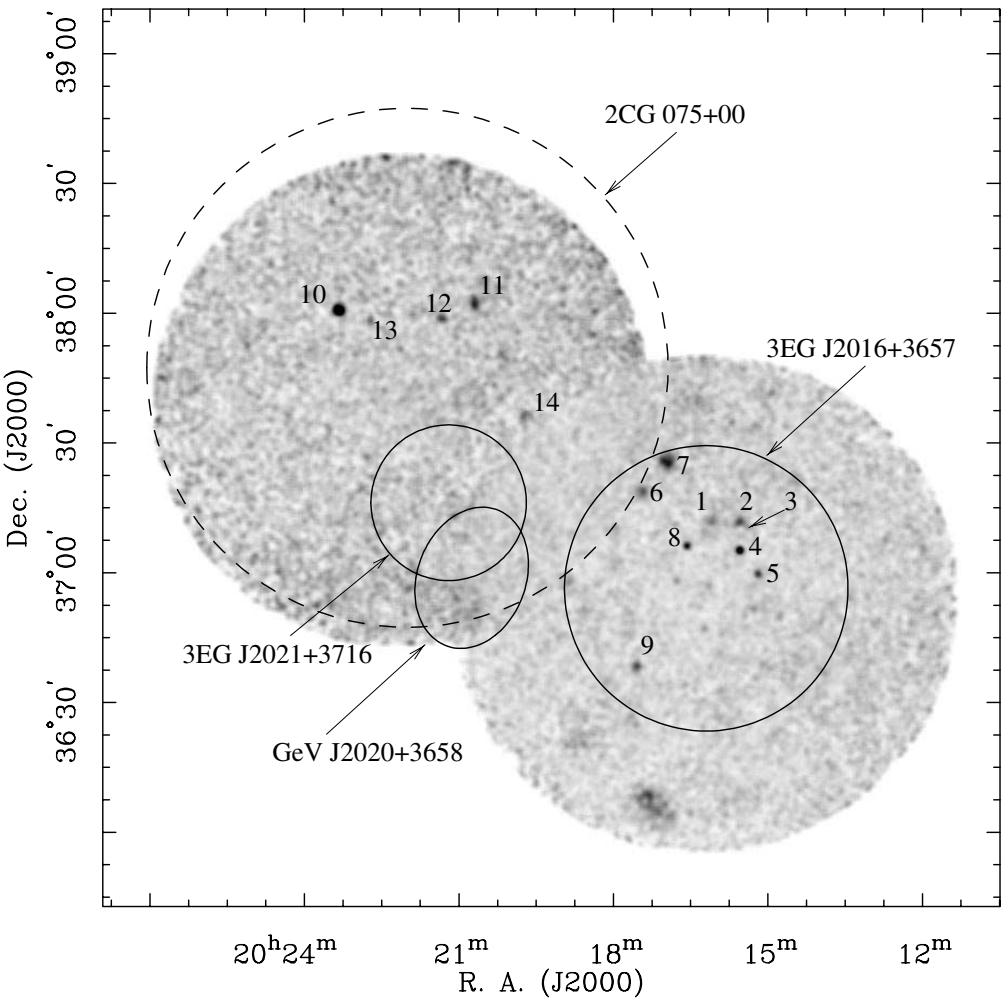

FIG. 1.—*ROSAT* soft X-ray image of 3EG J2016+3657 and 3EG J2021+3716. The circles for the two 3EG sources correspond to the ~95% confidence contours. The dashed circle corresponds to the *COS B* source 2CG 075+00. The GeV Catalog source is also shown.

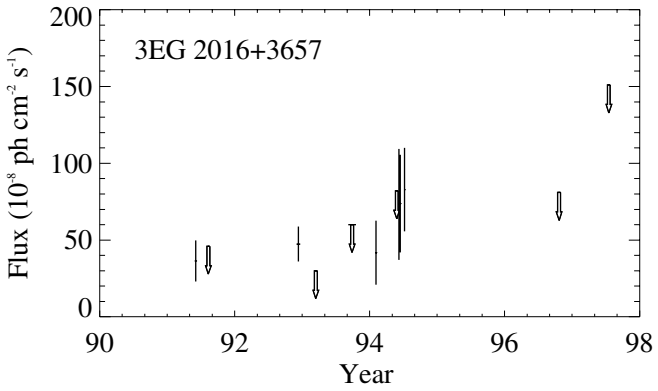

FIG. 2*a*

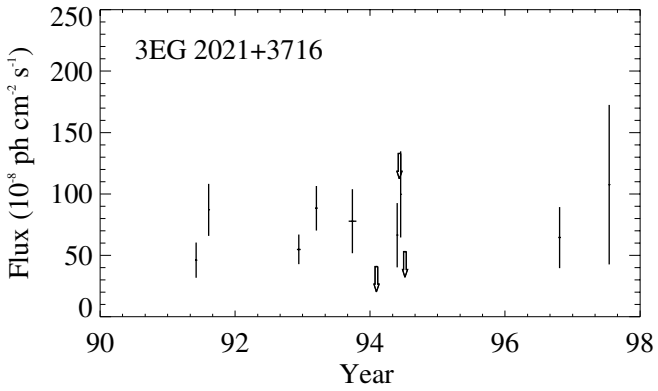

FIG. 2*b*

FIG. 2.—EGRET γ-ray light curves for (*a*) 3EG J2016+3657 and (*b*) 3EG J2021+3716 from 1991 to 1997. 2 σ upper limits are shown as arrows. The horizontal error bars correspond to the extent of an individual observation.

rather than being intrinsic to the sources. In comparison with the EGRET blazars, 3EG J2016+3657 and 3EG J2021+3716 have variability indices similar to a large fraction of the blazars detected by EGRET (Mukherjee et al. 1997b).

The background-subtracted γ-ray spectra of 3EG J2016+3657 and 3EG J2021+3716 were determined by dividing the EGRET energy band of 30 MeV–10 GeV into four bins for 3EG 2016+3657 and 10 bins for 3EG 2021+3716 and estimating the number of source photons in each interval, following the EGRET spectral analysis technique of Nolan et al. (1993). The data were fitted to a single power law of the form $F(E) \propto (E)^{-\Gamma}$ photons cm^{-2} s^{-1} MeV^{-1}, where $F(E)$ is the flux, E is the energy, and Γ is the photon spectral index. The photon spectral indices of 3EG J2016+3657 and 3EG J2021+3716 were found to be, respectively, 1.99 ± 0.20 and 1.86 ± 0.10.

3. THE X-RAY OBSERVATIONS

The error boxes of both 3EG sources are covered by archival X-ray imaging observations acquired with the *ROSAT* and *ASCA* observatories. Two adjacent observations with each observatory fall nicely on the two 3EG error boxes. Historically, these fields have been studied in X-rays because of the existence of both the 2CG source, as well as several known X-ray sources in the region. The *ASCA* observations herein were a part of a program to study unidentified sources in the Galactic plane (M. Tavani et al. 2000, in preparation).

Archival data for the region were available for the *ROSAT* Position Sensitive Proportional Counter (PSPC), the *ROSAT* High Resolution Imager (HRI), and the *ASCA* Gas Imaging Spectrometer (GIS), which allow complementary broadband X-ray data in the 0.2–2.0 keV (PSPC) and 1–10 keV (GIS) range with arcminute spatial resolution and moderate energy resolution. The PSPC 1° radius field of view is about twice that of the GIS. The *ROSAT* HRI observations took place on 1994 November 12–13, with a total exposure time of 43 ks. The *ROSAT* PSPC observations were on 1991 November 22–30, 1992 April 28–30, 1993 October 24–25, and 1994 June 5, with a total exposure time of $\sim$12 ks. The *ASCA* observations took place on 1995 May 29–31, 1995 October 14–15, and 1996 February 2. All data were obtained from the High-Energy Astrophysics Science Archive Research Center (HEASARC) archive at Goddard Space Flight Center and edited using the latest standard processing for each mission.

We created *ROSAT* (Fig. 1) and *ASCA* (Fig. 3) images of the region containing 3EG J2016+3657 and 3EG J2021+3716 by co-adding exposure-corrected sky maps from each mission. These images are centered on the position of the earlier Second Catalog source, 2EG 2019+3719. However, the PSPC image size is large enough to include the 95% error contours of both the 3EG sources. Note that the *ASCA* images are not centered on the EGRET positions and only part of the error contour of 3EG 2016+3657 is covered by the *ASCA* observation. In both Figure 1 and Figure 3 we show the error circles of 2CG 075+00 with dashed lines. Also shown is the error circle of the GeV source GeV J2020+2658 (Lamb & Macomb 1997).

To search for a possible X-ray counterpart to the γ-ray sources, we examined the *ROSAT* point sources enclosed by the 95% contours of the two 3EG sources. The detected positions are numbered in the image (Fig. 1) and are tabulated in Table 1. There are nine bright sources in the *ROSAT* image of 3EG J2016+3657 but none that are significant within the error circle of 3EG J2021+3716. Note that source 3 (indicated with an arrow) is very faint and barely resolved in the *ROSAT* PSPC image. Its position is determined from the *ROSAT* HRI image shown in § 4. There are at least five X-ray sources in the error circle of 2CG 075+00, which reached a minimum detectable intrinsic flux of 6.5×10^{-13} ergs cm^{-2} s^{-1} in the 0.1–2.4 keV band, assuming a power-law photon spectral index of 2.0 and a Galactic column absorption of 1×10^{22} cm^{-2}.

The *ASCA* images were, similarly, searched for corresponding X-ray counterparts. In deriving the *ASCA* positions, we were able to use the *ROSAT* point sources seen in the *ASCA* images to improve the astrometry for the *ASCA* sources to 10″ by registering the *ASCA* images using the overlapping *ROSAT* sources. There are no significant point sources in the *ASCA* image within the 95% contour of 3EG J2021+3716. The *ASCA* image of 3EG J2016+3657 reveals five point sources, which are indicated with numbers in Figure 3. Source numbers 1, 2, 3, 4, and 5 correspond to *ROSAT* sources of the same numbers in Figure 1.

To measure the *ASCA* and *ROSAT* source count rates we extracted photons using a 2′ radius aperture and esti-

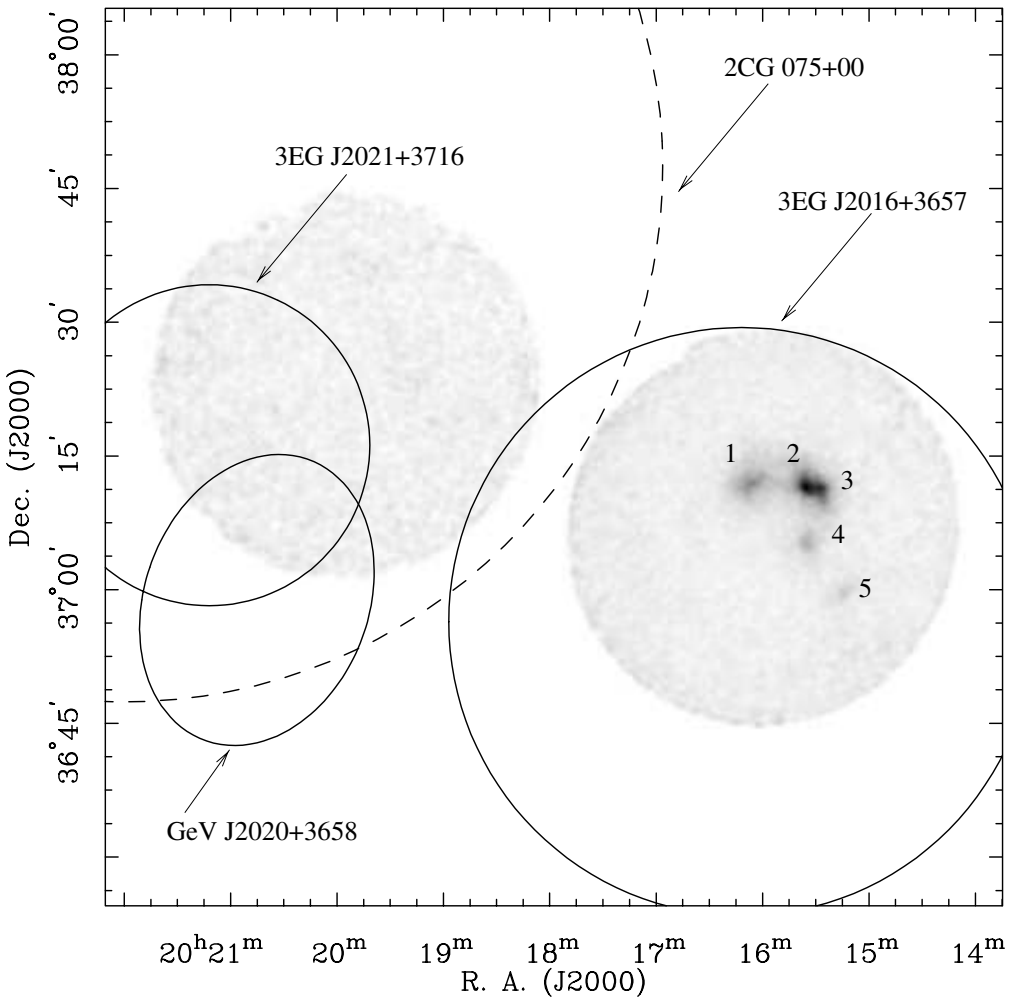

FIG. 3.—Same as Fig. 1 but for an *ASCA* image of 3EG J2016+3657 and 3EG J2021+3716

TABLE 1

X-RAY SOURCES IN THE FIELDS OF 3EG J2016+3657 AND 3EG J2021+3716

Number[a]	Source Name	R.A.	Decl.	Count Rate[b] (*ASCA*)	Hardness Ratio[c] (*ASCA*)	Significance[d] (*ASCA*)	Count Rate[b] (*ROSAT*)	Significance[d] (*ROSAT*)
1	CTB 87	20 16 11.5	+37 11 19	24 ± 0.7	−0.42	28	7.5 ± 1.6	4.3
2		20 15 36.6	+37 11 25	30 ± 0.7	...	42	8.8 ± 1.6	5.1
3	B2013+370	20 15 28.3	+37 11 02	15 ± 0.4	...	30	...	...
4		20 15 35.7	+37 04 59	9 ± 0.6	0.0	12	19.0 ± 2.1	8.8
5		20 15 14.9	+36 59 22	3 ± 0.4	−0.26	5.5	11.5 ± 1.8	6.1
6	HD 228766	20 17 29.0	+37 18 28	...	...	...	13.6 ± 1.8	7.3
7	HD 193077	20 16 59.8	+37 25 26	...	...	...	25.6 ± 2.2	11.1
8	Bright Star	20 16 37.4	+37 05 55	...	...	...	12.4 ± 1.8	6.5
9	Bright Star	20 17 34.6	+36 38 06	...	...	...	2.6 ± 9.1	2.4
10		20 23 22.2	+37 59 42	...	...	...	40.6 ± 3.8	10.6
11		20 20 42.4	+38 02 05	...	...	...	16.5 ± 3.0	5.2
12	CCDM J20215+3758A	20 21 21.6	+37 58 15	...	...	...	7.7 ± 2.4	3.0
13	HD 229153	20 22 45.7	+37 57 18	...	...	...	3.9 ± 2.0	2.0
14	Bright Star	20 19 43.7	+37 35 49	...	...	...	11.4 ± 1.8	4.4

NOTE.—Units of right ascension are hours, minutes, and seconds, and units of declination are degrees, arcminutes, and arcseconds.

[a] Identifying number in *ROSAT* image (Fig. 1).

[b] Background-subtracted source count rate $\times 10^{-3}$ s^{-1} extracted from a 2′ diameter aperture, in the 2–10 keV energy band for *ASCA* and the 0.5–2 keV energy band for *ROSAT* (PSPC).

[c] Hardness ratio (*ASCA*). For sources 2 and 3 this is not determined because of severe cross contamination.

[d] Significance computed using method of Gotthelf & Kaspi 1998.

mated the background contribution using a large annulus away from the other source following the method described in Gotthelf & Kaspi (1998). For *ASCA*, we define hardness ratio as

$$\frac{S(<2\text{ keV}) - S(>2\text{ keV})}{S(<2\text{ keV}) + S(>2\text{ keV})}.$$

The *ASCA* and *ROSAT* sources are listed in Table 1 along with their background-subtracted count rates, detection significances, and hardness ratios. We found no other point sources in the *ASCA* image at the level of 5 σ or higher other than those listed in Table 1.

We have searched for counterparts of the X-ray sources in the *ROSAT* and *ASCA* images. Several of the sources have optical identifications and are listed in Table 1. Source 1 is a known supernova remnant (SNR), CTB 87. Two of the sources can be identified with radio sources. Notes on the individual sources in Table 1 are given in the following section.

4. NOTES ON INDIVIDUAL SOURCES

CTB 87.—Source 1 in Table 1 is coincident with SNR CTB 87 (G74.9+1.2), an extended source with a flat radio spectrum. G74.9+1.2 is a filled-center SNR in the radio with high polarization and a high frequency turnover. Its H I absorption indicates a distance of 12 kpc. It has a relatively flat spectrum in the radio with a spectral index of 0.26 ± 0.2 below 11 GHz, beyond which a transition to a steeper spectral index occurs with the spectrum steepening to an index greater than 1. (Morsi & Reich 1987; Salter et al. 1989). It is generally believed that filled-center SNRs are remnants in which a central object is responsible for the relativistic electrons, whose synchrotron emission is detected at radio frequencies (Koyama et al. 1997). The flat radio spectrum is believed to be due to the central pulsar, which injects particles into the nebula (Reynolds & Chevalier 1984).

B2013+370.—The hard X-ray source marked "3" in the *ASCA* image (Fig. 3), which is barely resolved in the *ROSAT* PSPC image (Fig. 1), is consistent with the radio source B2013+370 (G74.87+1.22). B2013+370 is a well-studied compact, flat-spectrum radio source that was first noticed during the study of the SNR CTB 87 (Duin et al. 1975). It is located approximately 7′ west of the brightness peak of CTB 87. Wilson (1980) first noted the association of the radio source with an extended or possibly double X-ray source observed in the 0.15–3.0 keV band with the Imaging Proportional Counter (IPC) on the *Einstein Observatory*. The IPC source, 1E 2013.7+3701, was situated roughly between the locations of our sources 2 and 3. The *ROSAT* HRI image (Fig. 4), however, shows that the *Einstein* source is clearly resolved into two point sources, corresponding to sources 2 and 3.

Because of its proximity to the SNR, the possibility that B2013+370 and CTB 87 are related cannot be excluded. However, such an association is unlikely based on the requirements of an unprecedented velocity for the radio source if it were to be associated with the nearby SNR (see, e.g., the arguments presented in Shaffer et al. 1978).

In fact, B2013+370 has all the characteristics of a compact, extragalactic, nonthermal radio source and is typical of the many extragalactic sources seen by EGRET. Duin et al. (1975) report a radio spectral index of $\alpha = -0.2$ at high frequencies (above $\sim$7500 MHz) and a low-frequency spectral index of about $\alpha = +0.4 \pm 0.06$. The source exhibits a lack of recombination line emission, the presence of linear polarization, and a spectrum consistent with a nonthermal source showing synchrotron self-absorption below 8 GHz, as expected for a magnetic field of less than 0.1 G (Duin et al. 1975). VLBI measurements indicate an angular extent of less than 0.″001 at 8 GHz and greater than 0.″009 at 0.8 GHz (Weiler & Shaver 1978). From its radio properties, B2013+370 is very likely to be a flat-spectrum radio quasar or a BL Lac object. It has a 5 GHz flux of about 2 Jy (Duin et al. 1975), typical of many blazars seen by EGRET. In addition, B2013+370 is detected at 90 and 142 GHz with the IRAM 30 m telescope and exhibits variability at these wavelengths, a specific property of EGRET blazars (Bloom et al. 1999; Mattox et al. 1997). This is demonstrated in Figure 5, which shows the light curves of B2013+370 at 90 and 142 GHz, measured between 1993 and 1995 (Reuter et al. 1997).

HD 228766.—This is a Wolf-Rayet star, also known as SAO 69765 (Hog et al. 1998), and is the counterpart to source 6 in Table 1. It has a *B* magnitude of 9.72 and a *V* magnitude of 9.22. Its spectral type is O5.5f.

HD 193077.—Source 7 in Table 1 is a bright ($B = 8.34$, $V = 8.06$) Wolf-Rayet star, HD 193077 (Perryman et al. 1997), also known as SAO 69755. The star corresponds to WR 138 in the Wolf-Rayet catalog (van der Hucht et al. 1981). It is a star of the WN sequence (subtype WN5+OB), with its spectra dominated by broad emission lines of helium and nitrogen (Lepine & Moffat 1999).

CCDM J20215+3758A.—Together with CCDM J20215+3758B, this corresponds to a double star system and is the counterpart to source 12 in Table 1. The USNO-A2.0 catalog gives the magnitudes of the two stars as follows: CCDM J20215+3758A: $R = 11.6$, $B = 12.1$, and CCDM J20215+3758B: $R = 11.9$, $B = 13.5$.

HD 229153.— This is the counterpart to source 13 in Table 1 (Hog et al. 1998). It is a bright star ($B = 10.09$, $V = 9.14$) of spectral type B0 Iab.

We also find three of the other X-ray sources to be coincident with bright stars in the USNO-A2.0 catalog. Source 8 is possibly a star ($B = 12.4$, $R = 11.3$) with coordinates (J2000) $20^h16^m37^s.55$, $+37°05'55''.0$, and source 9 is most likely a star of approximately 12th magnitude at (J2000) $20^h17^m35^s.86$, $+36°38'02''.3$. Source 14 probably corresponds to a star ($B = 11.7$, $R = 10.8$) with coordinates (J2000) $20^h19^m44^s.16$, $+37°35'26''.7$. In addition, we find two point sources in the *ROSAT* HRI image (Fig. 4), not listed in Table 1, to be coincident with bright stars. These are marked in the figure as HD 228600 at (J2000) $20^h15^m30^s.8$, $+37°20'03''.1$ ($B = 10.5$, $V = 10.1$) and a star ($B = 15.7$, $R = 14.2$) at (J2000) $20^h16^m49^s.0$, $+36°57'48''$.

We do not find any likely counterparts in the literature to the other remaining sources in Table 1.

4.1. *Optical Observations*

We obtained CCD images in the *R* band using the 2.4 m telescope of the Michigan-Dartmouth-MIT (MDM) Observatory on 2000 April 24 and in the *I* band on March 18 using the MDM 1.3 m. The regions covered were $2' \times 2'$ on the 2.4 m and $8' \times 8'$ on the 1.3 m. In seeing of 0.″75, an optical object of $R = 21.6 \pm 0.2$ is detected at (J2000) $20^h15^m28^s.76$, $+37°10'59''.9$ in the USNO-A2.0 reference system (Monet et al. 1996), with an uncertainty of 0.″3. This

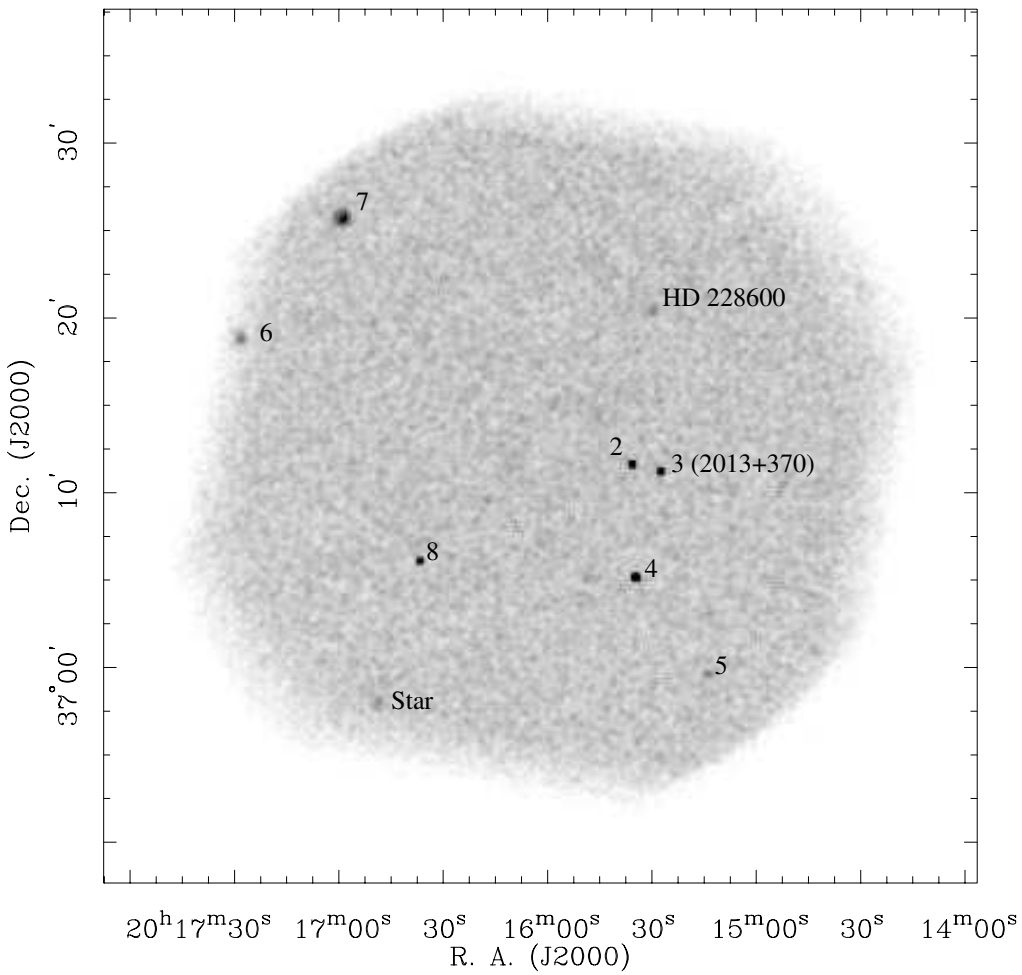

FIG. 4.—*ROSAT* HRI X-ray image of the field around 3EG J2016+3657. The image shows the sources 2 and 3 (B2013+370) as clearly resolved point sources. The image is scaled to highlight point features. The source numbers correspond to those listed in Table 1.

coincides with the NRAO/VLA Sky Survey (NVSS) position (Table 2) of the blazar B2013+370, identified with X-ray source 3, as shown in Figure 6. This object was also detected optically by Geldzahler, Shaffer, & Kühr (1984), who found $I = 19.5 \pm 0.5$ while also noting that it appeared extended. Our *R*-band image shows that the object closest to the radio position is unresolved while a fainter object 1.″7 to the northwest was almost certainly responsible for the extended appearance in the Geldzahler et al. (1984) image. Assuming standard conversions of N_H to extinction, the absorption in the *R* band is ≈ 5.1 mag to an extragalactic object, making its intrinsic magnitude $R = 16.5$. Our *I*-band images have inferior seeing, but they also detect the blended pair at the radio position, as well as optical objects at the positions of X-ray sources 2 and 4. However, in the absence of further information such as radio detection or optical spectroscopy, the severe crowding and Galactic extinction makes the identification of these additional X-ray sources by positional coincidence alone dangerous, even from HRI positions.

TABLE 2

RADIO SOURCES (>0.3 Jy) WITHIN THE ERROR CIRCLES OF 3EG J2016+3657 AND 3EG J2021+3716

NVSS 1.4 GHz		Integrated Flux		Integrated Flux	
R.A. (2000)	Decl. (2000)	(Jy)	WENSS (326 MHz) Name	(Jy)	Other Names
20 15 28.73.....	+37 10 59.9	2.17 ± 0.07	WNB 2013.6+3701	1.14	B2013+370
20 15 53.68.....	+37 11 30.2	1.02 ± 0.03	...	...	Associated with CTB 87
20 16 04.13.....	+37 12 23.5	1.81 ± 0.06	WNB 2014.1+3703	1.69	CTB 87
20 16 05.82.....	+37 14 05.5	1.17 ± 0.04	...	...	Associated with CTB 87
20 17 46.86.....	+36 44 47.9	0.29 ± 0.01	...	...	H II region S104
20 21 38.67.....	+37 31 10.1	6.58 ± 0.24	WNB 2019.7+3718B	1.49	H II region
20 21 41.60.....	+37 25 52.1	2.98 ± 0.11	WNB 2019.7+3718C	1.98	H II region

NOTE.—Units of right ascension are hours, minutes, and seconds, and units of declination are degrees, arcminutes, and arcseconds.

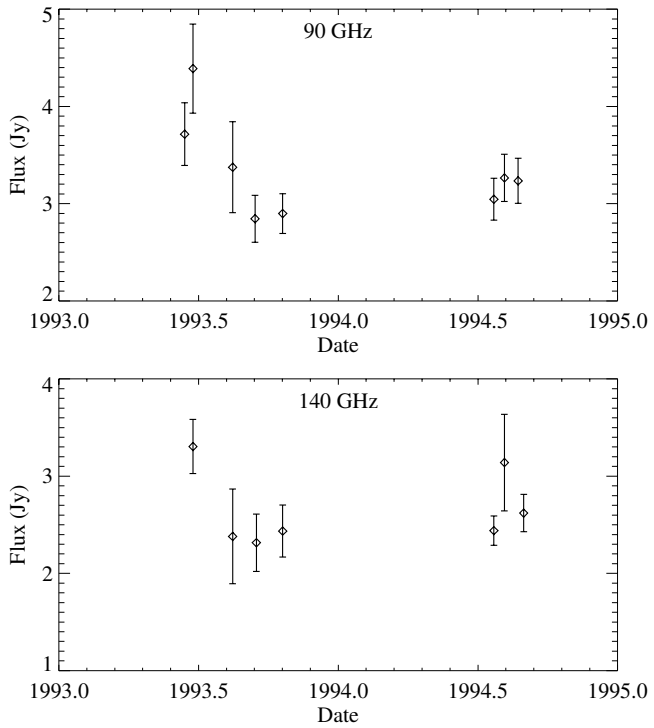

FIG. 5.—Flux history of B2013+370 at 90 and 140 GHz between 1993 and 1995 (data compiled from Reuter et al. 1997).

4.2. *Other Radio Sources*

We have searched the NVSS catalog (Condon et al. 1998) of 1.4 GHz radio sources for other possible counterparts to the X-ray and γ-ray sources. A search within the error box of 3EG J2016+3657 revealed 126 radio sources. Of these, only five had integrated radio fluxes greater than 0.3 Jy and are shown in Figure 7 and Table 2. The two brightest of these are positionally coincident with the *ROSAT* and *ASCA* sources 1 (CTB 87) and 3 (B2013+370). The two sources clustered near CTB 87 are actually extended regions within the supernova remnant. None of the other NVSS sources match the positions of the X-ray sources in the *ASCA* and *ROSAT* images.

There are two bright (>0.3 Jy) radio sources within the error circle of 3EG J2021+3716 (see Fig. 7, Table 2). Both of these were also detected by *IRAS* and were shown to be H II regions from their radio recombination lines (Lockman 1989).

A search of the Westerbork Northern Sky Survey (WENSS) catalog (Rengelink et al. 1997) of 92 cm (325 MHz) radio sources yielded similar results. This survey has a limiting flux density of about 18 mJy. A search within the error box of 3EG J2016+3657 yielded 21 radio sources, of which only two matched the positions of the X-ray sources. These are (*a*) WNB 2014.1+3703 positionally coincident with *ROSAT* and *ASCA* source 1, or CTB 87 and (*b*) WNB 2013.6+3701 matching the *ASCA* source 3, or B2013+370. A search within the error circle of 3EG J2021+3716 yielded a pair of very bright radio sources, WNB 2019.7+3718B and WNB 2019.7+3718C, which correspond to the H II regions also seen in the NVSS data (see Table 2).

5. DISCUSSION

Our study of archival X-ray (*ASCA* and *ROSAT*) data yields several faint sources within the error boxes of the two 3EG sources. The region contains bright stars, the SNR CTB 87, a compact radio source, and H II regions.

The presence of the SNR CTB 87 (G74.9+1.2) in the field of 3EG J2016+3657 is potentially quite important in light of the γ-ray source/SNR associations noticed in previous investigations (Sturner & Dermer 1995; Esposito et al. 1996). Gamma-ray production from SNRs, Wolf-Rayet stars, and OB associations is expected in several theoretical models. This subject was extensively investigated in the past for *COS B* sources (Montmerle 1979; Völk & Forman 1982) and recently for EGRET (Romero et al. 1999; Esposito et al. 1996; Kaaret & Cottam 1996). If the γ-ray emission were from a young pulsar associated with the SNR, a conclusive way to prove this would be to find pulsations. This is unfortunately not possible for such a weak X-ray source.

However, the energetics of the CTB 87 remnant are far from adequate to produce a source detectable by EGRET at the inferred distance of 12 kpc. Wilson (1980) argued convincingly that the X-ray luminosity of CTB 87, which is 100 times less than that of the Crab, implies that the spin-down power of the embedded pulsar must be correspondingly less, $I\Omega\dot{\Omega} \approx 1 \times 10^{36}(d/12 \text{ kpc})$ ergs s^{-1}. Even assuming that 100% of this power is emitted in the EGRET energy band, the resulting flux of 6×10^{-11} ergs cm^{-2} s^{-1} is 20 times less than the EGRET-measured average flux of 3EG J2016+3657. This argument is insensitive to distance as long as the X-ray synchrotron nebula is considered a calorimeter of the present pulsar power. If, instead, CTB 87 hosts a Geminga-like pulsar whose energy is no longer trapped by the nebula and is maximally efficient in the production of γ-rays, then we would expect a spin-down power of only $\sim 3 \times 10^{34}$ ergs s^{-1}. Such a pulsar is inadequate to explain the flux of 3EG J2016+3657 unless it were at $d < 500$ pc, which is certainly ruled out by the H I and X-ray–measured column density to the SNR. We believe that the SNR CTB 87 is an interesting Crab-like remnant but is too weak and too far away to be a good candidate for the EGRET source 3EG J2016+3657.

Similarly, neither the bright stars in the X-ray images nor the H II regions are likely to be responsible for the EGRET source.

We believe that the most likely candidate for 3EG J2016+3657 is the radio source B2013+370, described in § 4. Based on its radio properties B2013+370 is very likely to be a blazar, similar to the others seen by EGRET. Mattox et al. (1997) find that only the brightest radio-flat active galactic nuclei (AGNs) can be identified with EGRET sources with any level of confidence and demonstrate that there is a high degree of correlation between γ-ray and radio fluxes of EGRET blazars. EGRET has detected more than 65 AGNs (Hartman et al. 1999), almost all of which can be classified as blazars. The blazars seen by EGRET all share the common characteristic that they are radio-loud, flat-spectrum sources, with radio spectral indices $0.6 > \alpha > -0.6$ (von Montigny et al. 1995). Several of these blazars exhibit superluminal motion of components resolved with VLBI (e. g., 3C 279, 3C 273, PKS 0528+134). The blazar class of AGN includes highly polarized quasars, BL Lac objects, or optically violent variable (OVV) quasars. The sources are characterized by one or more properties of this source class, namely, a flat radio spectrum, a continuum spectrum that is nonthermal, optical polarization, and strong variability. For most EGRET blazars, the γ-ray luminosity dominates that at other wave bands.

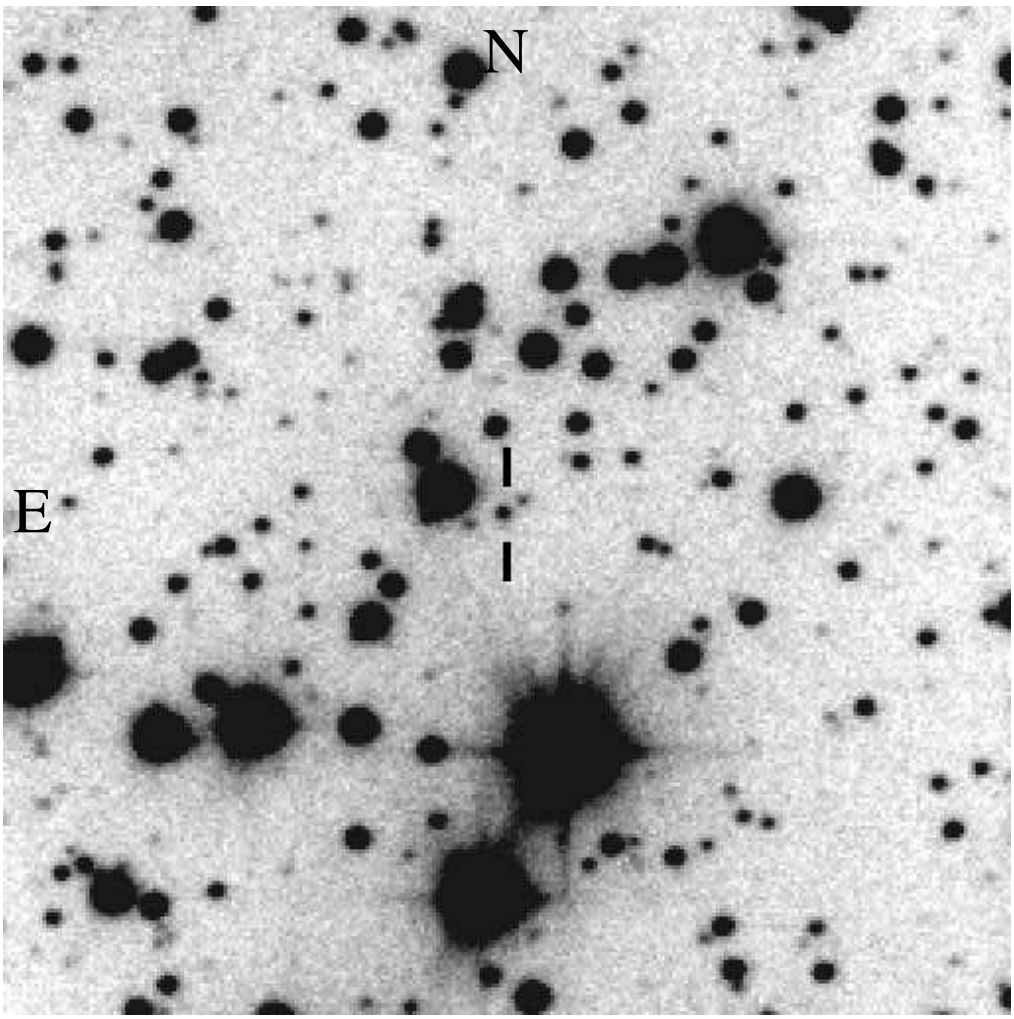

FIG. 6.—Section of the combined *R*-band CCD images from the MDM 2.4 m telescope. Total exposure time was 30 minutes. The field shown is 70″ × 70″. Tick marks are centered on the NVSS position of the blazar B2013+370. The optical object between the tick marks has $R = 21.6 \pm 0.2$ and is located at (J2000) $20^h15^m28^s.76$, $+37°10'59''.9$.

The probability that the blazar B2013+370 is the correct identification for the EGRET source 3EG J2016+3657 can be estimated by following the calculations presented by Mattox et al. (1997). The a priori probability that EGRET will detect a random flat-spectrum blazar with a 5 GHz flux of 2 Jy is 5.8% (Mattox et al. 1997). However, since in this case there is an EGRET source at this location, the conditional (a posteriori) probability must be used, which takes into account the fact that a γ-ray source has already been detected. The a posteriori probability that a blazar of the type that we see in the error circle of an EGRET source is in fact the correct identification is about 98.8%. The factors that enter into this calculation are the radio flux (2 Jy) and spectral index (+0.3), the 95% error radius of the EGRET source (0°.55), the distance of the radio source from the center of the EGRET circle (0°.27), and the mean distance between radio sources that are at least as strong and at least as flat as this one (~16°.7.)

Figure 8 shows the spectral energy distribution of B2013+370, assuming that it is the EGRET source 3EG J2016+3657. The figure shows the relative amounts of energy detected in equal logarithmic frequency ranges. The radio fluxes were obtained from the NRAO/VLA Sky Survey, the Westerbork Northern Sky Survey (see § 4.2), and a compilation of radio fluxes in Weiler & Shaver (1978). The fluxes at millimeter wavelengths were obtained from Reuter et al. (1997), taken with the IRAM 30 m telescope. The optical point was measured by us at the MDM Observatory and has been corrected for extinction (§ 4.1). The estimated unabsorbed X-ray flux for source 3 (=B2013+370) in the *ASCA* band of 1–10 keV is $(6 \pm 1) \times 10^{-13}$ ergs cm^{-2} s^{-1} and in the *ROSAT* band of 0.1–2.4 keV is $(1.9 \pm 0.2) \times 10^{-12}$ ergs cm^{-2} s^{-1}. For the flux estimations we have assumed $N_H = 10^{22}$ cm^{-2} and a power-law photon index of 2. The data in Figure 8 are not contemporaneous. The EGRET spectrum was derived as explained in § 2.

The broadband spectrum shown in Figure 8 is that of a typical EGRET blazar, dominated by the power output in γ-rays. The spectrum shows the characteristic features of a blazar, with a synchrotron peak at lower energies and an inverse Compton peak at higher energies. The high γ-ray luminosity of a blazar suggests that the emission is likely to be beamed and, therefore, Doppler boosted along the line of sight. In this scenario, synchrotron radiation from high-energy electrons in a relativistically outflowing jet are responsible for the radio to UV continuum. The high-energy photons come from inverse Compton scattering of

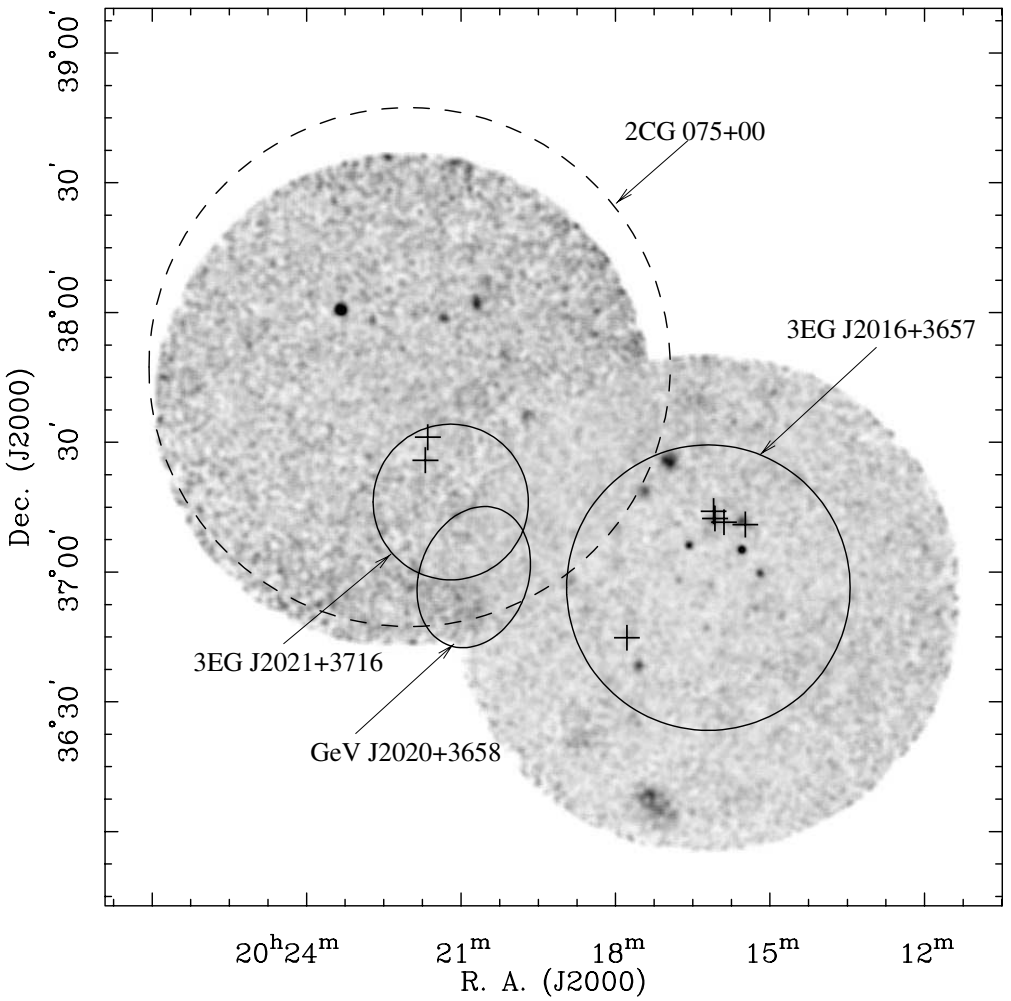

FIG. 7.—*ROSAT* PSPC image of 3EG J2016+3657 and 3EG J2021+3716 showing the bright 1.4 GHz radio sources from the NRAO/VLA Sky Survey within the error circles of the EGRET sources. Only those sources with radio fluxes greater than 0.3 Jy are shown. Refer to Table 2 for fluxes and source positions. The error circles of 2CG 075+00, the two EGRET catalog sources, and the GeV Catalog source are indicated.

low-energy photons by the same relativistic electrons in the jet. Details of this model remain unresolved (e.g., see Hartman et al. 1997 for a review). The relative power output in γ-rays for B2013+370 is less than that of a typical flat-spectrum radio quasar seen by EGRET and is more similar to that observed in BL Lac objects. The location of the broad synchrotron peak in the optical-IR band rather than in the X-ray band is an indication that B2013+370 could be a low-energy–peaked BL Lac object (LBL), according to the classification suggested by Giommi & Padovani (1994).

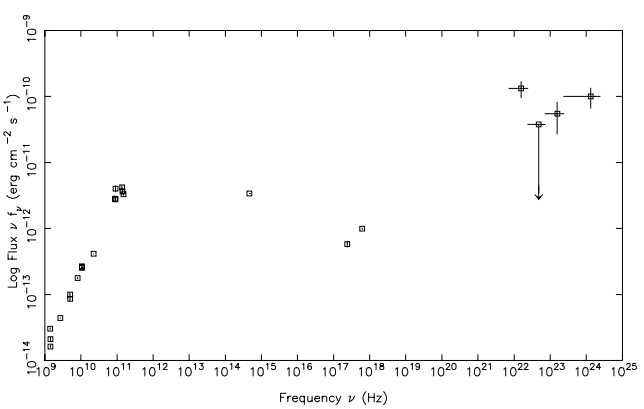

FIG. 8.—Broadband spectrum of B2013+370, assuming that it is the γ-ray source 3EG J2016+3657.

We believe that the association of 3EG J2016+3657 with B2013+370 is real and that the source of both is most likely a blazar.

In conclusion, we have made a comprehensive study of the X-ray and γ-ray sources in the error circle of the *COS B* source 2CG 075+00. We have identified most of the X-ray sources in the error boxes of the EGRET sources. One reasonable hypothesis is that 2CG 075+00 is largely the same source as 3EG J2021+3716 and that 3EG J2016+3657 is a new source, which can be identified with the radio blazar 2013+3710 = X-ray source 3. Herein 2CG 075+00 = 3EG J2021+3716 remains unidentified. Clearly, for the 3EG sources considered here, we need more refined γ-ray positions and extensive monitoring (possibly by *AGILE* and *GLAST*) to establish their ultimate nature.

We thank Jonathan Kemp for obtaining optical images at MDM Observatory. We acknowledge support by NASA grant NAG5-3696 (R. M.), NASA grant NAG5-7935 (E. V. G.), and NASA grant NAG5-3229 (J. P. H). This research has made use of data obtained from HEASARC at Goddard Space Flight Center and the SIMBAD astronomical database.

REFERENCES

Bertsch, D. L., et al. 1992, Nature, 357, 306
Bloom, S. D., Marscher, A. P., Moore, E. M., Gear, W., Teräsranta, H., Valtaoja, E., Aller, H. D., & Aller, M. 1999, ApJS, 122, 1
Brazier, K. T. S., Kanbach, G., Carraminana, A., Guichard, J., & Merck, M. 1996, MNRAS, 281, 1033
Brazier, K. T. S., Reimer, O., Kanbach, G., & Carraminana, A. 1998, MNRAS, 295, 819
Condon, J. J., Cotton, W. D., Greisen, E. W., Yin, Q. F., Perley, R. A., Taylor, G. B., & Broderick, J. J. 1998, AJ, 115, 1693
Duin, R. M., Israel, F. P., Dickel, J. R., & Seaquist, E. R. 1975, A&A, 38, 461
Esposito, J. A., et al. 1996, ApJ, 461, 820
———. 1999, ApJS, 123, 203
Geldzahler, B. J., Shaffer, D. B., & Kühr, H. 1984, ApJ, 286, 284
Giommi, P., & Padovani, P. 1994, MNRAS, 268, L51
Gotthelf, E. V., & Kaspi, V. 1998, ApJ, 497, L29
Hartman, R. C., Collmar, W., von Montigny, C., & Dermer, C. D. 1997, in AIP Conf. Proc. 410, Proc. 4th Compton Symp., ed. C. D. Dermer, M. S. Strickman, & J. D. Kurfess (New York: AIP), 307
Hartman, R. C., et al. 1999, ApJS, 123, 79
Hog, E., Kuzmin, A., Bastian, U., Fabricius, C., Kuimov, K., Lindegren, L., Makarov, V. V., & Roeser, S. 1998, A&A, 335, L65
Kaaret, P., & Cottam, J. 1996, ApJ, 462, L35
Kaspi, V. M., Lackey, J. R., Mattox, J., Manchester, R. N., Bailes, M., & Pace, R. 2000, ApJ, 528, 445
Kaul, R. K., & Mitra, A. K. 1997, in AIP Conf. Proc. 410, Proc. 4th Compton Symp., ed. C. D. Dermer, M. S. Strickman, & J. D. Kurfess (New York: AIP), 1271
Koyama, K., Kinugasa, K., Matsuzaki, K., Nishiuchi, M., Sugizaki, M., Torii, K., Yamauchi, S., & Aschenbach, B. 1997, PASJ, 49, L7
Lamb, R. C., & Macomb, D. J. 1997, ApJ, 488, 872
Lepine, S., & Moffat, A. F. J. 1999, ApJ, 514, 909
Lockman, F. J. 1989, ApJS, 71, 469
Mattox, J. R., Schachter, J., Molnar, L., Hartman, R. C., & Patnaik, A. R. 1997, ApJ, 481, 95
Mattox, J. R., et al. 1996, ApJ, 461, 396
McLaughlin, M. A., et al. 1996, ApJ, 473, 763
Mirabal, N., Halpern, J. P., Eracleous, M., & Becker, R. H. 2000, ApJ, 541, 180
Monet, D., et al. 1996, USNO-SA2.0 (Washington DC: US Naval Observatory)
Montmerle, T. 1979, ApJ, 231, 95
Morsi, H. W., & Reich, W. 1987, A&AS, 69, 533
Mukherjee, R., Grenier, I. A., & Thompson, D. J. 1997a, in AIP Conf. Proc. 410, Proc. 4th Compton Symp., ed. C. D. Dermer, M. S. Strickman, & J. D. Kurfess (New York: AIP), 384
Mukherjee, R., et al. 1997b, ApJ, 490, 116
Nolan, P., et al. 1993, ApJ, 409, 697
Ozël, M. E., Schlickeiser, R., Sieber, W., & Younis, S. 1988, A&A, 200, 195
Perryman, M., et al. 1997, A&A, 323, L49
Pollock, A. M. T., et al. 1985, A&A, 146, 352
Rengelink, R. B., Tang, Y., de Bruyn, A. G., Miley, G. K., Bremer, M. N., Roettgering, H. J. A., & Bremer, M. A. R. 1997, A&AS, 124, 259
Reynolds, S. P., & Chevalier, R. A. 1984, ApJ, 278, 630
Reuter, H.-P., et al. 1997, A&AS, 122, 271
Roberts, M. S. E., & Romani, R. W. 1998, ApJ, 496, 827
Romero, G. E., Benaglia, P., & Torres, D. F. 1999, preprint (astro-ph/9904355)
Salter, C. J., Reynolds, S. P., Hogg, D. E., Payne, J. M., & Rhodes, P. J. 1989, ApJ, 338, 171
Shaffer, D. B., Geldzahler, B. J., Kellermann, K. I., Pauliny-Toth, I. I. K., Preuss, E., & Witzel, A. 1978, A&A, 68, L11
Sturner, S. J., & Dermer, C. D. 1995, A&A, 293, L17
Swanenburg, B. N., et al. 1981, ApJ, 243, L69
Thompson, D. J., et al. 1992, Nature, 359, 615
———. 1993, ApJS, 86, 629
———. 1995, ApJS, 101, 259
van der Hucht, K. A., Conti, P. S., Lundstrom, I., & Stenholm, B. 1981, Space Sci. Rev., 28, 307
Völk, H. J., & Forman, M. 1982, ApJ, 253, 188
von Montigny, C., et al. 1995, A&A, 299, 680
Weiler, K. W., & Shaver, P. A. 1978, A&A, 70, 389
Wilson, A. S. 1980, ApJ, 241, L19
Yadigaroglu, I.-A., & Romani, R. W. 1997, ApJ, 476, 347